A Conservative and Monotone Mixed–Hybridized Finite Element Approximation of Transport Problems in Heterogeneous Domains

Marco Brera, [a] Joseph W. Jerome, [b] Yoichiro Mori, [c]
Riccardo Sacco [d]

[a] *Master Degree in Electronic Engineering, Politecnico di Milano*
Piazza Leonardo da Vinci 32, 20133 Milano, Italy

[b] *Department of Mathematics, Northwestern University*
2033 Sheridan Road, Evanston, IL 60208-2730, USA

[c] *School of Mathematics, University of Minnesota,*
206 Church Street, Minneapolis, MN 55455, USA

[d] *Dipartimento di Matematica "F. Brioschi", Politecnico di Milano*
via Bonardi 9, 20133 Milano, Italy

Abstract

In this article, we discuss the numerical approximation of transport phenomena occurring at material interfaces between physical subdomains with heterogenous properties. The model in each subdomain consists of a partial differential equation with diffusive, convective and reactive terms, the coupling between each subdomain being realized through an interface transmission condition of Robin type. The numerical approximation of the problem in the two–dimensional case is carried out through a dual mixed–hybridized finite element method with numerical quadrature of the mass flux matrix. The resulting method is a conservative finite volume scheme over triangular grids, for which a discrete maximum principle is proved under the assumption that the mesh is of Delaunay type in the interior of the domain and of weakly acute type along the domain external boundary and internal interface. The stability, accuracy and robustness of the proposed method are validated on several numerical examples motivated by applications in Biology, Electrophysiology and Neuroelectronics.

Key words: Transport phenomena, heterogeneous problems, mixed–hybridized finite element methods, electrophysiology, neuroelectronics, mathematical modeling, numerical simulation.

* Corresponding author: Riccardo Sacco
Email address: riccardo.sacco@polimi.it (Riccardo Sacco).

1 Introduction and Motivation

In this article, we deal with the numerical approximation of the following Diffusion-Advection-Reaction (DAR) model problem with gradient advective field:
Find $u \in \mathcal{H}^1(\Omega)$ such that:

$$\begin{cases} \mathcal{L}u = \text{div}\, \boldsymbol{J}(u) + c\, u = f & \text{in } \Omega \\ \boldsymbol{J}(u) = -D\,(\boldsymbol{\nabla} u + u\, \boldsymbol{\nabla}\psi) & \text{in } \Omega \\ u = u_D & \text{on } \Gamma_D \\ \boldsymbol{J}(u)\cdot \boldsymbol{n} = \gamma\, u + j_R & \text{on } \Gamma_R \\ \boldsymbol{J}(u)\cdot \boldsymbol{n}_1 = \alpha\, u_1 - \beta\, u_2 + \sigma_1 & \text{on } \Gamma_{m,1} \\ \boldsymbol{J}(u)\cdot \boldsymbol{n}_2 = \beta\, u_2 - \alpha\, u_1 - \sigma_2 & \text{on } \Gamma_{m,2}, \end{cases} \tag{1}$$

where $\Omega = \Omega_1 \cup \Omega_2$ is an open bounded set of $\mathbb{R}^2$ with Lipschitz boundary $\partial\Omega \equiv \Gamma$, an example of which is depicted in Fig.1, while $\mathcal{H}^1(\Omega) := \prod_{i=1}^{2} H^1(\Omega_i)$ is the "broken" space of functions belonging to $L^2(\Omega)$ whose gradient is piecewise square integrable over Ω, u_i being the restriction of the solution $u : \Omega \to \mathbb{R}$ to the subdomain Ω_i, $i = 1, 2$. The domain boundary Γ is partitioned into the disjoint segments

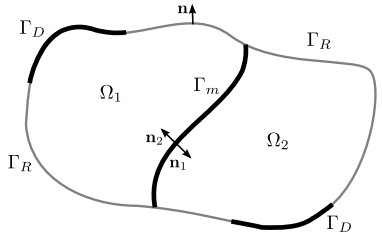

Figure 1. Computational domain with material interface.

Γ_D and Γ_R, where the Dirichlet boundary condition $(1)_3$ and the Robin boundary condition $(1)_4$ are enforced, and an internal interface Γ_m, where the transmission conditions $(1)_{5,6}$ are enforced. We indicate by $\Gamma_{m,1}$ and $\Gamma_{m,2}$ the restrictions of Γ_m when viewed from Ω_1 and Ω_2, respectively, while the outward unit normal vectors to Γ, $\Gamma_{m,1}$ and $\Gamma_{m,2}$ are $\boldsymbol{n}$, $\boldsymbol{n}_1$ and $\boldsymbol{n}_2$, respectively. The quantity $D \in L^\infty(\Omega)$ is the diffusion coefficient, with $D(\boldsymbol{x}) \geq D_{min} > 0$ almost everywhere (a.e.) in Ω, while $c \in L^\infty(\Omega)$ is the reaction coefficient, with $c(\boldsymbol{x}) \geq 0$ a.e. in Ω. The vector $\boldsymbol{\nabla}\psi$ is a given advective field in gradient form, and the regularity of the generating potential function ψ will be specified in Sect.3. Finally, $f \in L^2(\Omega)$ is the production term and $\boldsymbol{J}(u)$ is the advective-diffusive flux density associated with the scalar variable u. Boundary and interface data u_D, γ, j_R, α, β, σ_1 and σ_2 are given functions whose regularity will be made precise in Sect.3, u_D being > 0 and α, β, γ being ≥ 0.

Well posedness of the linear system (1) can be proved by adapting the ideas of Ref. [49]. The model problem (1) is representative of several important applica-

tions, ranging from electrokinetic flows in nanofluidics [56,2] to cell biology [40,1]. A common feature of these applications is the presence of active interfaces (membranes) whose selective behavior controls mass transport from a subdomain to the neighbouring one according to the difference between the values of the electrostatic potential ψ across the membrane. In this work, ψ is assumed to be a given function, but in realistic situations, for example in the study of current flux across ionic channels using the so-called Poisson-Nernst-Planck (PNP) model [56], the potential is itself an unknown of the problem and is dynamically determined by the solution of Gauss' law in differential form in the domain Ω supplied by interface conditions across Γ_m similar to $(1)_{5,6}$. Time advancing in PNP simulations is typically treated using Rothe's method and, at each semi-discrete time level, the nonlinear coupling between the dependent variables u and ψ is usually dealt with by some suitable functional iteration of decoupled type [36,37,49,43,39,38] which eventually leads to the successive solution of linearized systems of the form (1).

Equation $(1)_1$ is a conservation law expressing the balance between the flux of the advective–diffusive vector field $\boldsymbol{J}(u)$ across an arbitrary control volume $\mathcal{B} \subseteq \Omega$ and the production term $f - c\,u$ within the volume itself. In particular, the jump of the normal component of $\boldsymbol{J}(u)$ is equal to zero across each segment belonging to the interior of Ω_1 and Ω_2, respectively, while it is equal to $\sigma_1 - \sigma_2$ across the membrane Γ_m, as it can be checked by summing $(1)_5$ and $(1)_6$. Using the terminology of Computational Mechanics, where u has the meaning of displacement and $\boldsymbol{J}(u)$ is the stress field, it is well-known that standard displacement-based finite element methods for the numerical approximation of (1) generally fail at satisfying the above properties, despite the optimal convergence of the approximate solution u_h to u in the H^1-norm (see [51]). An effective alternative is represented by dual mixed (DM) methods, where two *independent* discrete solutions u_h and $\boldsymbol{J}_h$ are simultaneously sought for, leading to a linear system in saddle-point form. DM methods satisfy both local self-equilibrium and conservation, and an optimal error estimate holds for the pair (u_h, $\boldsymbol{J}_h$) in the graph norm with respect to the L^2-$H(\mathrm{div})$ topology (see [14]). However, there are several drawbacks that make them not so amenable to realistic computations, namely, the increased computational cost, the indefinite algebraic character of the system, and a possible failure at satisfying the discrete maximum principle (DMP) for u_h in the case of a nonvanishing reaction term c (see [16] and references cited therein). A considerable improvement consists of resorting to the *hybridization* of the DM formulation (see, [4] and [14], Chapt. V; for more recent development in the framework of Discontinuous Gakerkin methods, see also [23]). The hybridization procedure is based on the introduction of a Lagrange multiplier denoted by λ_h (hybrid variable), which is an approximation of u along mesh edges and allows one to enforce the interelement continuity of the normal component of $\boldsymbol{J}_h$. The local elimination of the variables u_h and $\boldsymbol{J}_h$ as functions of λ_h (static condensation) leads to a dual mixed–hybridized (DMH) finite element scheme of displacement–based type, acting on the sole λ_h, which is completely equivalent to the original DM approximation but at a much reduced computational effort. Moreover, it can be shown that the hybrid variable enjoys su-

perconvergence properties. However, the question of ensuring a numerically stable computed solution in the presence of dominating convection and/or reaction terms still remains an open issue, and appropriate stabilization techniques must be used (see [16,15] and the more recent work [23]). To this end, we propose in this article a finite volume variation of the standard DMH method, denoted DMH-FV method, based on the introduction of a quadrature formula for the diagonalization of the local flux mass matrix. This approach, that extends to the heterogeneous transport problem (1) previously introduced MFV formulations [3,11,45,16], has three important advantages. The first is that the resulting numerical scheme has a simple and very compact finite volume structure where for each element of the grid, the computational stencil consists of the element itself and, at most, its three neighbours. The second is that the treatment of the exponentially varying diffusion coefficient across inter-element edges allows, under mild geometric conditions, a DMP for the computed discrete solution. The third is that the novel method enjoys the same convergence properties as the standard DMH scheme, including superconvergence in the L^2-norm of the post-processed solution obtained from λ_h (see [4]).

A brief outline of the article is as follows. In Sect. 2, we introduce the geometric entities and finite element spaces; in Sect. 3, we first introduce the change of variable that allows one to write problem (1) in symmetric form. Then, we describe the DMH-FV method, while in Sect. 4 we illustrate the computer implementation of the scheme and related post-processing. Sect. 5 contains a thorough validation of the numerical performance of the novel scheme, and Sect. 6 addresses some concluding remarks and future research perspectives.

2 Geometric Discretization and Finite Element Spaces

Let $\{\mathcal{T}_h\}$ be a regular family of given partitions of the domain Ω into open triangles K satisfying the usual admissibility condition (see [51], Sect. 3.1 and Def. 3.4.1). For a given $\mathcal{T}_h$, we denote by $\mathtt{NT}$ and $\mathtt{Ne}$ the total number of triangles and edges, respectively, by $|K|$ and h_K the area and the diameter of K, respectively, and we set $h = \max_{\mathcal{T}_h} h_K$. Let $\boldsymbol{x} = (x, y)^T$ be the position vector in Ω; then, for each $K \in \mathcal{T}_h$, we denote by $\boldsymbol{x}_q$, $q = 1, 2, 3$, the three vertices of K ordered according to a counterclockwise orientation, by $\boldsymbol{e}_q$ the edge of ∂K which is opposite to $\boldsymbol{x}_q$, by θ_q^K the angle opposite to $\boldsymbol{e}_q$ and by C_K the circumcenter of K. We denote by $|\boldsymbol{e}_q|$ the length of $\boldsymbol{e}_q$ and by $\boldsymbol{n}_q$ the outward unit normal vector along $\boldsymbol{e}_q$. Moreover, we define s_q^K as the signed distance between C_K and the midpoint M_q of $\boldsymbol{e}_q$. If $\theta_q^K < \pi/2$ then $s_q^K > 0$, while if K is obtuse in θ_q^K then $s_q^K < 0$, and C_K falls outside K. Notice also that if $\theta_q^K = \pi/2$ then $s_q^K = 0$, and C_K coincides with M_q. We denote by $\mathcal{E}_h$ the set of edges of $\mathcal{T}_h$, and by $\mathcal{E}_{h,int}$ and $\mathcal{E}_{h,\Gamma}$ those belonging to the interior of Ω and to the boundary Γ, respectively. For each $e \in \mathcal{E}_{h,int}$, we indicate by K_e^1 and K_e^2 the pair of elements of $\mathcal{T}_h$ such that $e = \partial K_e^1 \cap \partial K_e^2$. Finally, we let $s_e = s_e^{K_e^1} + s_e^{K_e^2}$ denote the signed distance between $C_{K_e^1}$ and $C_{K_e^2}$. If $\theta_e^{K_e^1} + \theta_e^{K_e^2} < \pi$

for all $e \in \mathcal{E}_{h,int}$, then $s_e > 0$, and $\mathcal{T}_h$ is called a *Delaunay triangulation* [30]. If the inequality is replaced by an equality, for some $e \in \mathcal{E}_{h,int}$, we call $\mathcal{T}_h$ a *degenerate Delaunay triangulation*. For such an edge, $s_e = 0$ and the two circumcenters $C_{K_e^1}$, $C_{K_e^2}$ collapse into the midpoint of e. The Delaunay condition prevents the occurrence of pairs of *obtuse* neighbouring elements in $\mathcal{T}_h$, still allowing the possibility of having single obtuse triangles in the computational grid (see [31] for algorithmic details). From now on, we assume that $\mathcal{T}_h$ is a Delaunay triangulation.
For $k \geq 0$ and a given set $\mathcal{S}$, we denote by $\mathbb{P}_k(\mathcal{S})$ the space of polynomials of degree $\leq k$ defined over $\mathcal{S}$. We also denote by $\mathbb{R}T_0(K) := (\mathbb{P}_0(K))^2 \oplus \mathbb{P}_0(K)\,\boldsymbol{x}$ the Raviart–Thomas (RT) finite element space of lowest degree [52], and by $\mathcal{P}_0$ the L^2-projection over constant functions. Then, for $g \in L^2(\Gamma_D)$, we introduce the following finite element spaces:

$$\begin{aligned}
\mathbf{V}_h &:= \{\boldsymbol{v} \in (L^2(\Omega))^2 \,|\, \boldsymbol{v}^K \in \mathbb{R}T_0(K)\ \forall K \in \mathcal{T}_h\} \\
W_h &:= \{w \in L^2(\Omega) \,|\, w^K \in \mathbb{P}_0(K)\ \forall K \in \mathcal{T}_h\} \\
M_{h,g} &:= \{m \in L^2(\mathcal{E}_h) \,|\, m|_{\partial K} \in \mathcal{R}_0(\partial K) \forall K \in \mathcal{T}_h, \\
&\qquad m^{K_e^1} = m^{K_e^2}\ \forall e \in \mathcal{E}_{h,int},\ m^e = \mathcal{P}_0 g|_e, \forall e \in \Gamma_D\},
\end{aligned} \tag{2}$$

where $\mathcal{R}_0(\partial K) := \{v \in L^2(\partial K) |\ v|_e \in \mathbb{P}_0(e)\ \forall e \in \partial K\}$. For each $K \in \mathcal{T}_h$, the basis functions of $\mathbb{R}T_0(K)$ are $\boldsymbol{\tau}_j(\boldsymbol{x}) = (\boldsymbol{x} - \boldsymbol{x}_j)/(2|K|)$, $j = 1, 2, 3$, and are such that $\operatorname{div} \boldsymbol{\tau}_j = 1/|K|$ and $\boldsymbol{\tau}_j \cdot \boldsymbol{n}_j = 1/|\boldsymbol{e}_j|$ for each $\boldsymbol{e}_j \in \partial K$, which implies that $\int_{e_j} \boldsymbol{\tau}_i \cdot \boldsymbol{n}_j \, d\varsigma = \delta_{ij}$, $i, j = 1, 2, 3$, δ_{ij} being the Kronecker symbol. Functions belonging to $M_{h,g}$ are single-valued on $\mathcal{E}_{h,int} \cup \Gamma_D \cup \Gamma_R$, while they admit two distinct values on each edge $e \in \Gamma_m$. This latter, special, situation reproduces, on the discrete level, the selectivity characteristic of the membrane Γ_m, and allows accounting for the occurrence of finite jump discontinuities across Γ_m. It is also useful to introduce the following global finite element space

$$\begin{aligned}
\Lambda_h = \{&v_h \in L^2(\Omega) \,|\, v_h \in \mathbb{P}_1(K)\ \forall K \in \mathcal{T}_h, \\
&v_h(M_e^{K_e^1}) = v_h(M_e^{K_e^2})\ \forall e \in \mathcal{E}_{h,int}\} = \operatorname{span}\{\omega_e\}_{e \in \mathcal{E}_h},
\end{aligned}$$

where the basis functions ω_e are the non-conforming elements of Crouzeix-Raviart [28]. Functions in Λ_h are piecewise linear over $\mathcal{T}_h$, continuous at the midpoint of each edge $e \in \mathcal{E}_{h,int}$ and possibly admitting a finite jump discontinuity at each edge $e \in \Gamma_m$.

3 A Mixed–Hybridized Method with Numerical Quadrature

With the aim of constructing a finite element approximation of the DAR model problem (1), we introduce the change of dependent variable

$$u := \rho\, e^{-\psi}. \tag{3}$$

The idea, proposed originally in [10] and subsequently used in [19] for the numerical treatment with mixed methods of the Drift-Diffusion semiconductor device equations, consists of using (3) to write (1) in symmetric form, then, to discretize the new equivalent problem with a proper (finite volume) modification of the DMH method, and, finally, to go back to the original variable u via (3) again on the discrete level. This gives a numerical scheme for the approximation of (1) whose stiffness matrix is an M-matrix under mild assumptions on the computational grid.

The change of variable (3) transforms the original advection–diffusion–reaction system (1) into the equivalent problem of finding the solution $\rho \in \mathcal{H}^1(\Omega)$ of the following linear diffusion-reaction model problem in conservative form:

$$\begin{cases} \mathcal{L}\rho = \text{div } \boldsymbol{J}(\rho) + c\,\rho\,e^{-\psi} = f & \text{in } \Omega \\ \boldsymbol{J}(\rho) = -D\,e^{-\psi}\boldsymbol{\nabla}\rho & \text{in } \Omega \\ \rho = \rho_D & \text{on } \Gamma_D \\ \boldsymbol{J}(\rho)\cdot\boldsymbol{n} = \gamma\,\rho\,e^{-\psi} + j_R & \text{on } \Gamma_R \\ \boldsymbol{J}(\rho)\cdot\boldsymbol{n}_1 = \alpha\,\rho_1\,e^{-\psi_1} - \beta\,\rho_2\,e^{-\psi_2} + \sigma_1 & \text{on } \Gamma_{m,1} \\ \boldsymbol{J}(\rho)\cdot\boldsymbol{n}_2 = \beta\,\rho_2\,e^{-\psi_2} - \alpha\,\rho_1\,e^{-\psi_1} - \sigma_2 & \text{on } \Gamma_{m,2}, \end{cases} \tag{4}$$

where $\rho_D := u_D\,e^{\psi_D}$ and $\psi_D := \psi|_{\Gamma_D}$. Comparing (4) with (1), we see that the use of relation (3) has transformed the original DAR problem into a new equivalent diffusion-reaction problem with an exponentially varying diffusion coefficient $D\,e^{-\psi}$ and a new dependent variable ρ. From now on, we assume that D, c and f are piecewise constant given functions over $\mathcal{T}_h$, and that ρ_D, γ and j_R are piecewise constant boundary data over $\mathcal{E}_{h,\Gamma}$, with the same assumption for the transmission coefficients α, β, σ_1 and σ_2, and that $\psi \in \Lambda_h$. Moreover, given a function η, we denote by η^K and η_e the constant values of η over each element $K \in \mathcal{T}_h$ and each edge $e \in \mathcal{E}_h$, respectively. Finally, we set for brevity $a := D\,e^{-\psi}$ and $A := a^{-1}$.

The DMH Galerkin approximation of problem (4) consists of finding $(\boldsymbol{J}_h,\, \rho_h,\, \lambda_h) \in (\mathbf{V}_h \times W_h \times M_{h,\rho_D})$ such that:

$$\begin{cases} (A\,\boldsymbol{J}_h,\, \boldsymbol{\tau}_h)_{\mathcal{T}_h} - (\rho_h,\, \text{div}\,\boldsymbol{\tau}_h)_{\mathcal{T}_h} + \langle \lambda_h,\, \boldsymbol{\tau}_h\cdot\boldsymbol{n}\rangle_{\mathcal{E}_h} = 0 & \forall \boldsymbol{\tau}_h \in \mathbf{V}_h \\ (\text{div}\,\boldsymbol{J}_h + c\,e^{-\psi}\,\rho_h,\, q_h)_{\mathcal{T}_h} = (f,\, q_h)_{\mathcal{T}_h} & \forall q_h \in W_h \\ \langle \boldsymbol{J}_h\cdot\boldsymbol{n},\, \mu_h\rangle_{\mathcal{E}_h} = \langle \gamma\,\lambda_h\,e^{-\psi},\, \mu_h\rangle_{\Gamma_R} + \langle j_R,\, \mu_h\rangle_{\Gamma_R} & \\ \quad + \langle \alpha\,\lambda_h\,e^{-\psi_1},\, \mu_h\rangle_{\Gamma_{m,1}} - \langle \beta\,\lambda_h\,e^{-\psi_2},\, \mu_h\rangle_{\Gamma_{m,1}} & \\ \quad + \langle \sigma_1,\, \mu_h\rangle_{\Gamma_{m,1}} + \langle \beta\,\lambda_h\,e^{-\psi_2},\, \mu_h\rangle_{\Gamma_{m,2}} & \\ \quad - \langle \alpha\,\lambda_h\,e^{-\psi_1},\, \mu_h\rangle_{\Gamma_{m,2}} - \langle \sigma_2,\, \mu_h\rangle_{\Gamma_{m,1}} & \forall \mu_h \in M_{h,0}, \end{cases} \tag{5}$$

where $(\cdot,\,\cdot)_{\mathcal{T}_h}$ and $\langle\cdot,\,\cdot\rangle_{\mathcal{S}}$ denote the elementwise L^2 inner products over $\mathcal{T}_h$ and

over any subset $\mathcal{S} \subseteq \mathcal{E}_h$, respectively. The equations in (5) have the following interpretation: $(5)_1$ expresses the approximate local constitutive law; $(5)_2$ expresses the approximate local balance between net flux across K and net production of mass inside K; $(5)_3$ expresses the approximate continuity of $\boldsymbol{J} \cdot \boldsymbol{n}$ across each interelement edge, the Robin boundary condition and the interface transmission condition. The approximate interelement continuity of ρ and the Dirichlet boundary condition are automatically expressed by the fact that λ_h is a single–valued function over $\mathcal{E}_{h,int} \cup \Gamma_D \cup \Gamma_R$. Using the static condensation procedure allows one to eliminate u_h and $\boldsymbol{J}_h$ in favor of the sole hybrid variable λ_h and leads to solving a linear algebraic system whose size is of the order of `Ne`, which makes the DMH formulation a generalized displacement-based method. Once λ_h is available, the variables u_h and $\boldsymbol{J}_h$ can be recovered by post-processing over each mesh element. The DMH formulation was originally proposed and theoretically analyzed in [4] in the study of an elliptic model problem with Dirichlet boundary conditions. Further analysis and extensions can be found in [14,53,54]. Related approaches in the framework of Discontinuous Galerkin methods have been recently proposed and analyzed in the series of papers [24,25,22,26,27,23].

To construct a DMH scheme with reduced computational effort, we proceed as follows. For each $K \in \mathcal{T}_h$, we set

$$\boldsymbol{J}_h^K(\boldsymbol{x}) = \sum_{j=1}^{3} \Phi_j^K \, \boldsymbol{\tau}_j(\boldsymbol{x}) \qquad \boldsymbol{x} \in K, \tag{6}$$

where the degree of freedom $\Phi_j^K = \int_{e_j} \boldsymbol{J}_h^K \cdot \boldsymbol{n}_j \mathrm{d}\zeta$ is the flux of $\boldsymbol{J}_h^K$ across edge $\boldsymbol{e}_j$, $j = 1, 2, 3$. Then, we consider the following quadrature formula

$$\begin{aligned} &\int_K A \, \boldsymbol{J}_h^K \cdot \boldsymbol{\tau}_i \mathrm{d}K = \sum_{j=1}^{3} \Phi_j^K \int_K A \, \boldsymbol{\tau}_j \cdot \boldsymbol{\tau}_i \mathrm{d}K \\ &\simeq \frac{1}{2} \Phi_j^K \overline{A}_i^K \cot(\theta_i^K) \delta_{ij} = \Phi_j^K \overline{A}_i^K \, \frac{s_i^K}{|\boldsymbol{e}_i|} \delta_{ij} \quad i, j = 1, 2, 3, \end{aligned} \tag{7}$$

where $\overline{A}_i^K := \int_{C_K}^{M_i} A^K(\zeta) \mathrm{d}\zeta / |s_i^K|$. Using the fact that $\psi \in \mathbb{P}_1(K)$, we have

$$\overline{A}_i^K = \frac{\int_{C_K}^{M_i} D^{-1}(\zeta) e^{\psi(\zeta)} \mathrm{d}\zeta}{|s_i^K|} = \frac{1}{\overline{D_i}^K} \frac{e^{\psi_i}}{Be\,(\psi^K - \psi_i)} \tag{8}$$

where $Be(t) := t/(e^t - 1)$ is the inverse of the Bernoulli function, and $\overline{D_i}^K$ is the constant value of the diffusion coefficient along the segment $\overline{C_K \, M_i}$ defined as:

$$\overline{D_i}^K = \begin{cases} D^K & \text{if } s_i^K \geq 0 \\ D^{K_i} & \text{if } s_i^K < 0. \end{cases} \tag{9}$$

The above definition is consistent with physical intuition, because in the case where $s_i^K < 0$ (i.e., $\theta_i^K > \pi/2$) the path of the integral in (8) lies completely in K_i, so that the diffusion coefficient that must be used to compute the average $\overline{A}_i^K$ is that associated with triangle K_i (opposite to K with respect to edge e_i). Using (9) makes the average $\overline{A}_i^K$ always a strictly positive quantity. Moreover, it can be shown that the diagonalization formula (7) is affected by the following quadrature error

$$\left| \int_K A\,\boldsymbol{\tau}_j \cdot \boldsymbol{\tau}_i \mathrm{d}K - \overline{A}_i^K \, \frac{s_i^K}{|\boldsymbol{e}_i|}\delta_{ij} \right| \leq C h_K \|\boldsymbol{\tau}_i\|_{H(\mathrm{div}\,;K)} \|\boldsymbol{\tau}_j\|_{H(\mathrm{div}\,;K)}, \tag{10}$$

where $H(\mathrm{div}\,;K) = \{\boldsymbol{\tau} \in (L^2(K))^2 \,|\, \mathrm{div}\,\boldsymbol{\tau} \in L^2(K)\ K \in \mathcal{T}_h\}$ and C is a positive constant depending on A and on the mesh regularity (see [45,16] for a proof).

Using (7) into $(5)_1$, we obtain the following discrete equations for the DMH method with diagonalized local mass flux matrix.

- Equation $(5)_1$:

$$\overline{A}_i^K \, \Phi_i^K \frac{s_i^K}{|\boldsymbol{e}_i|} - \rho^K + \lambda_i^K = 0 \qquad \forall K \in \mathcal{T}_h \qquad i = 1,2,3. \tag{11}$$

- Equation $(5)_2$:

$$\sum_{i=1}^{3} \Phi_i^K + c^K e^{-\psi^K} \rho^K |K| = f^K |K| \qquad \forall K \in \mathcal{T}_h. \tag{12}$$

- Equation $(5)_3$:

$$\Phi_e^{K_e^1} = \begin{cases} -\Phi_e^{K_e^2} & e \in \mathcal{E}_{h,int} \\ \left(\gamma_e\, \lambda_e\, e^{-\psi_e} + j_{R\,e}\right) |\boldsymbol{e}| & e \in \Gamma_R \\ \left(\alpha_e \lambda_{e,1}\, e^{-\psi_{e,1}} - \beta_e \lambda_{e,2}\, e^{-\psi_{e,2}} + \sigma_{e,1}\right) |\boldsymbol{e}| & e \in \Gamma_{m,1} \\ \left(\beta_e \lambda_{e,2}\, e^{-\psi_{e,2}} - \alpha_e \lambda_{e,1}\, e^{-\psi_{e,1}} - \sigma_{e,2}\right) |\boldsymbol{e}| & e \in \Gamma_{m,2}. \end{cases} \tag{13}$$

Equation (12) is already in genuine FV form, so that, to construct a finite volume approximation starting from system (11)–(13), we need to express the flux Φ_i^K as a function of ρ^K and ρ^{K_i}, for each $K \in \mathcal{T}_h$ and $i = 1,2,3$, proceeding as follows.

(Step 1). Consider equation (11) and assume that $\theta_i^K \neq \pi/2$. Then, for each $K \in \mathcal{T}_h$ we obtain the explicit relation

$$\Phi_i^K = -(\overline{A}_i^K)^{-1} \, \frac{\lambda_i^K - \rho^K}{s_i^K} |\boldsymbol{e}_i| \qquad i = 1,2,3. \tag{14}$$

In the special case where $\theta_i^K = \pi/2$, then $s_i^K = 0$ and equation (11) yields $\rho^K = \lambda_i^K$ irrespective of the (undetermined) value of Φ_i^K. Such a value can be

recovered by post-processing the computed solution ρ_h by using (11) as

$$\Phi_i^K = (f^K - c^K e^{-\psi^K} \rho^K)\,|K| - \sum_{j=1, j\neq i}^{3} \Phi_j^K. \tag{15}$$

(Step 2). For each $e \in \mathcal{E}_{h,int}$ we replace (14) into $(13)_1$, obtaining the explicit relation

$$\lambda_e = \frac{(\overline{A}_i^{K_e^1}\, s_i^{K_e^1})^{-1} \rho^{K_e^1} + (\overline{A}_i^{K_e^2}\, s_i^{K_e^2})^{-1} \rho^{K_e^2}}{(\overline{A}_i^{K_e^1}\, s_i^{K_e^1})^{-1} + (\overline{A}_i^{K_e^2}\, s_i^{K_e^2})^{-1}}. \tag{16}$$

Let $\mathcal{L}_e$ be the "lumping region" connecting $C_{K_e^1}$, $C_{K_e^2}$ and the two endpoints of e (the shaded area in Fig. 2). Then, introducing the *harmonic average* of a over

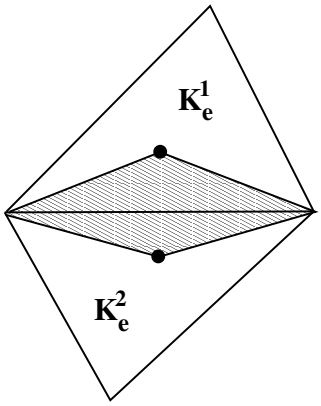

Figure 2. Lumping region $\mathcal{L}_e$.

$\mathcal{L}_e$, defined as

$$\mathcal{H}_e(a) := \left(\frac{\int_{s_e} a^{-1}(\zeta)\, d\zeta}{s_e} \right)^{-1} = \frac{s_e}{\overline{A}_i^{K_e^1}\, s_i^{K_e^1} + \overline{A}_i^{K_e^2}\, s_i^{K_e^2}},$$

we can write (16) in a more expressive manner as

$$\lambda_e = \mathcal{H}_e(a) \left(\overline{A}_i^{K_e^2} \frac{s_i^{K_e^2}}{s_e} \rho^{K_e^1} + \overline{A}_i^{K_e^1} \frac{s_i^{K_e^1}}{s_e} \rho^{K_e^2} \right) \equiv \mathcal{C}_e^1\, \rho^{K_e^1} + \mathcal{C}_e^2\, \rho^{K_e^2}. \tag{17}$$

The two constants $\mathcal{C}_e^1$ and $\mathcal{C}_e^2$ are such that $\mathcal{C}_e^1 + \mathcal{C}_e^2 = 1$. This ensures that the average (17) is consistent, i.e., if we set $\rho^{K_e^1} = \rho^{K_e^2} = \overline{\rho}$, then we get $\lambda_e = \overline{\rho}$, as should be expected. Using (8) over K_e^1 and K_e^2, we have

$$\mathcal{H}_e(a) = e^{-\psi_e} \frac{s_e}{\zeta_e^1 + \zeta_e^2}, \tag{18}$$

where $\zeta_e^r = s_i^{K_e^r} / \left(\overline{D}_i^{K_e^r}\, Be(\Delta\psi^{K_e^r}) \right)$ and $\Delta\psi^{K_e^r} := (\psi^{K_e^r} - \psi_e)$, $r = 1, 2$. The harmonic average (18) is a positive quantity, because $s_e > 0$ and $(\zeta_e^1 + \zeta_e^2) > 0$ due to the fact that $\mathcal{T}_h$ is a Delaunay triangulation and (9), respectively. For a discussion of the use of the harmonic average in the finite element approximation

of elliptic problems, and of its impact on the computational performance of the method, we refer to [5,4].

(Step 3). Substituting back (17) into (14) yields for each $K \in \mathcal{T}_h$ the explicit relation

$$\begin{aligned}\Phi_i^K &= -(\overline{A}_i^K)^{-1}\,\mathcal{C}_i^{K_i}\frac{\rho^{K_i}-\rho^K}{s_i^K}|\boldsymbol{e}_i| = -(\overline{A}_i^K)^{-1}\,\frac{\overline{A}_i^K\,s_i^K}{s_i}\mathcal{H}_{e_i}(a)\,\frac{\rho^{K_i}-\rho^K}{s_i^K}|\boldsymbol{e}_i| \\ &= -\mathcal{H}_{e_i}(a)\frac{\rho^{K_i}-\rho^K}{s_i}|\boldsymbol{e}_i| \qquad \forall \boldsymbol{e}_i \in \partial K \cap \mathcal{E}_{h,int}.\end{aligned} \tag{19}$$

The finite volume nature of the formulation proposed in the present article can be clearly recognized by comparison of the approximate flux Φ_i^K with the exact flux $\int_{e_i} -a\boldsymbol{\nabla}\rho\cdot\boldsymbol{n}_i\,ds$, which shows that the effect of the quadrature formula (7) is to replace the term $-(\boldsymbol{\nabla}\rho\cdot\boldsymbol{n}_i)|_{\mathcal{L}_{e_i}}$ with the incremental ratio $-(\rho^{K_i}-\rho^K)/s_i$ and the diffusion coefficient $a|_{\mathcal{L}_{e_i}}$ with its harmonic average $\mathcal{H}_{e_i}(a)$. This result extends to the dual mixed finite element setting the approach proposed in [47] for the Petrov-Galerkin finite element discretization of the convection-diffusion-reaction equation.

(Step 4). Equation (19) already relates the unknown ρ^K to the neighbouring unknowns ρ^{K_i}, then to complete the derivation of the finite volume scheme, we need to consider the case where $\boldsymbol{e}_i \in \Gamma$. We have:

$\boldsymbol{e}_i \in \Gamma_D$**:** in this case, combining (14) and (19) immediately yields

$$\Phi_i^K = -\mathcal{H}_{e_i}(a)\frac{\rho_D-\rho^K}{s_i^K}|\boldsymbol{e}_i|. \tag{20}$$

$\boldsymbol{e}_i \in \Gamma_R$**:** in this case, equating (14) with $(13)_2$ and eliminating the hybrid variable λ_{e_i}, yields

$$\Phi_i^K = \frac{\gamma_i\,e^{-\psi_i}\,\rho^K + j_{Ri}}{\overline{A}_i^K\,\gamma_i\,e^{-\psi_i}\,s_i^K + 1}|\boldsymbol{e}_i|. \tag{21}$$

$\boldsymbol{e}_i \in \Gamma_m$**:** in this case, combining relations (11) and $(13)_{3,4}$ and eliminating the hybrid variables $\lambda_{e,1}$ and $\lambda_{e,2}$, we get:

$$\begin{aligned}\Phi_i^{K_{e_i}^1} &= \frac{\alpha_i\,e^{-\psi_{i,1}}\,\rho^{K_{e_i}^1} - \beta_i\,e^{-\psi_{i,2}}\,\rho^{K_{e_i}^2} + \sigma_{i,1} + \overline{A}_i^{K_{e_i}^2}\,s_i^{K_{e_i}^2}\beta_i e^{-\psi_{i,2}}(\sigma_{i,1}-\sigma_{i,2})}{1+\overline{A}_i^{K_{e_i}^1}\,s_i^{K_{e_i}^1}\alpha_i e^{-\psi_{i,1}} + \overline{A}_i^{K_{e_i}^2}\,s_i^{K_{e_i}^2}\beta_i e^{-\psi_{i,2}}}|\boldsymbol{e}_i| \\ \Phi_i^{K_{e_i}^2} &= \frac{\beta_i\,e^{-\psi_{i,2}}\,\rho^{K_{e_i}^2} - \alpha_i\,e^{-\psi_{i,1}}\,\rho^{K_{e_i}^1} - \sigma_{i,2} + \overline{A}_i^{K_{e_i}^1}\,s_i^{K_{e_i}^1}\alpha_i e^{-\psi_{i,1}}(\sigma_{i,1}-\sigma_{i,2})}{1+\overline{A}_i^{K_{e_i}^1}\,s_i^{K_{e_i}^1}\alpha_i e^{-\psi_{i,1}} + \overline{A}_i^{K_{e_i}^2}\,s_i^{K_{e_i}^2}\beta_i e^{-\psi_{i,2}}}|\boldsymbol{e}_i|.\end{aligned} \tag{22}$$

Replacing the expression of the flux Φ_i^K into the equilibrium equation (12), we obtain the following linear system of algebraic equations that characterize the DMH-

FV approximation of problem (4)

$$\mathbf{A}^{\rho}\,\boldsymbol{\rho} = \mathbf{f} \tag{23}$$

where $\mathbf{A}^{\rho} \in \mathbb{R}^{\mathtt{NE}\times\mathtt{NE}}$ is the stiffness matrix, $\boldsymbol{\rho} \in \mathbb{R}^{\mathtt{NE}}$ is the unknown vector and $\mathbf{f} \in \mathbb{R}^{\mathtt{NE}}$ is the load vector, accounting for the contribution of the source function f and of the boundary and interface data. To write down the entries of $\mathbf{A}^{\rho}$ and $\mathbf{f}$, we indicate by $\mathtt{I}_K$ and $\mathtt{J}_{K_i}$ the global indices of element K and K_i, $i = 1, 2, 3$. Moreover, for each $K \in \mathcal{T}_h$, we introduce the non-negative quantities $\mathcal{N}_D^K$, $\mathcal{N}_R^K$ and $\mathcal{N}_m^K$ representing the number of edges of K which belong to Γ_D, Γ_R and Γ_m, respectively. Clearly, these quantities are all equal to zero if $\partial K \cap \Gamma = \emptyset$. Then, the diagonal entries of $\mathbf{A}^{\rho}$ read:

$$\begin{aligned}
A^{\rho}_{\mathtt{I}_K\mathtt{I}_K} &= \sum_{i=1}^{3} \xi_i^K + c^K e^{-\psi^K}|K| \\
\xi_i^K \quad &= \begin{cases}
\mathcal{H}_{e_i}(a)\dfrac{|\boldsymbol{e}_i|}{s_i} & \boldsymbol{e}_i \in \mathcal{E}_{h,int} \\
\mathcal{H}_{e_i}(a)\dfrac{|\boldsymbol{e}_i|}{s_i^K} & \boldsymbol{e}_i \in \Gamma_D \\
\dfrac{\gamma_i\, e^{-\psi_i}}{1 + \overline{A}_i^K \gamma_i\, e^{-\psi_i}\, s_i^K}|\boldsymbol{e}_i| & \boldsymbol{e}_i \in \Gamma_R \\
\dfrac{\alpha_i\, e^{-\psi_{i,1}}}{1 + \overline{A}_i^{K_{e_i}^1} s_i^{K_{e_i}^1} \alpha_i e^{-\psi_{i,1}} + \overline{A}_i^{K_{e_i}^2} s_i^{K_{e_i}^2} \beta_i e^{-\psi_{i,2}}}|\boldsymbol{e}_i| & \boldsymbol{e}_i \in \Gamma_{m,1} \\
\dfrac{\beta_i\, e^{-\psi_{i,2}}}{1 + \overline{A}_i^{K_{e_i}^1} s_i^{K_{e_i}^1} \alpha_i e^{-\psi_{i,1}} + \overline{A}_i^{K_{e_i}^2} s_i^{K_{e_i}^2} \beta_i e^{-\psi_{i,2}}}|\boldsymbol{e}_i| & \boldsymbol{e}_i \in \Gamma_{m,2},
\end{cases}
\end{aligned} \tag{24}$$

the off-diagonal entries of $\mathbf{A}^{\rho}$ are:

$$A^{\rho}_{\mathtt{I}_K\mathtt{J}_{K_i}} = \begin{cases}
-\mathcal{H}_{e_i}(a)\dfrac{|\boldsymbol{e}_i|}{s_i} & \boldsymbol{e}_i \in \mathcal{E}_{h,int} \\
-\dfrac{\beta_i\, e^{-\psi_{i,2}}}{1 + \overline{A}_i^{K_{e_i}^1} s_i^{K_{e_i}^1} \alpha_i e^{-\psi_{i,1}} + \overline{A}_i^{K_{e_i}^2} s_i^{K_{e_i}^2} \beta_i e^{-\psi_{i,2}}}|\boldsymbol{e}_i| & \boldsymbol{e}_i \in \Gamma_{m,1} \\
-\dfrac{\alpha_i\, e^{-\psi_{i,1}}}{1 + \overline{A}_i^{K_{e_i}^1} s_i^{K_{e_i}^1} \alpha_i e^{-\psi_{i,1}} + \overline{A}_i^{K_{e_i}^2} s_i^{K_{e_i}^2} \beta_i e^{-\psi_{i,2}}}|\boldsymbol{e}_i| & \boldsymbol{e}_i \in \Gamma_{m,2},
\end{cases} \tag{25}$$

and the load vector entries are:

$$
\begin{aligned}
f^u_{\mathtt{I}_K} &= f^K|K| + \sum_{i=1}^{\mathcal{N}_D^K} \eta_i^{K,D} + \sum_{i=1}^{\mathcal{N}_R^K} \eta_i^{K,R} + \sum_{i=1}^{\mathcal{N}_m^K} \eta_i^{K,m} \\
\eta_i^{K,D} &= \frac{u_{Di}}{\zeta_i^K}|\boldsymbol{e}_i| \\
\eta_i^{K,R} &= \frac{j_{Ri}}{1+\gamma_i\,\zeta_i^K}|\boldsymbol{e}_i| \\
\eta_i^{1,m} &= -\frac{\sigma_{i,1} + \beta_i\,\zeta_i^2\,(\sigma_{i,1}-\sigma_{i,2})}{1+\alpha_i\,\zeta_i^1+\beta_i\,\zeta_i^2}|\boldsymbol{e}_i| \\
\eta_i^{2,m} &= \frac{\sigma_{i,2} + \alpha_i\,\zeta_i^1\,(\sigma_{i,2}-\sigma_{i,1})}{1+\alpha_i\,\zeta_i^1+\beta_i\,\zeta_i^2}|\boldsymbol{e}_i|.
\end{aligned}
\tag{26}
$$

Some remarks about the properties of the numerical formulation illustrated in this section are in order.

The first remark concerns the algebraic properties of the DMH-FV method. Matrix $\mathbf{A}^\rho$ has, at most, four non–zero entries on each row, and is structurally symmetric, i.e., if $\mathbf{A}^\rho_{ij} \neq 0$ then also $\mathbf{A}^\rho_{ji} \neq 0$. In particular, denoting for each $e \in \mathcal{E}_{h,int}$ by $\mathtt{I}$ and $\mathtt{J}$ the indices of the two triangles such that $e = \partial K_\mathtt{I} \cap \partial K_\mathtt{J}$, we have that $\mathbf{A}^\rho_{\mathtt{IJ}} = \mathbf{A}^\rho_{\mathtt{JI}}$ if $e \in \mathcal{E}_{h,int} \backslash \Gamma_m$ while $\mathbf{A}^\rho_{\mathtt{IJ}} \neq \mathbf{A}^\rho_{\mathtt{JI}}$ if $e \in \Gamma_m$. The lack of symmetry numerically translates the nonsymmetric action of the transmission conditions $(4)_{5,6}$ with respect to the neighbouring subdomains Ω_1 and Ω_2. To make this issue more precise, we associate with each edge $e_i \in \Gamma_m$ the following "transmission" matrix $\mathbf{T}^\rho_i \in \mathbb{R}^{\mathtt{NE}\times\mathtt{NE}}$

$$
\mathbf{T}^\rho_i = \frac{|\boldsymbol{e}_i|}{\Delta_i}
\begin{array}{c}
\begin{matrix} \qquad\qquad\quad \mathtt{I} \qquad\qquad\quad \mathtt{J} \end{matrix} \\
\begin{bmatrix}
\ddots & & & 0 \\
 & \alpha_i e^{-\psi_{i,1}} & -\beta_i e^{-\psi_{i,2}} & \\
 & \ddots & & \\
 & -\alpha_i e^{-\psi_{i,1}} & \beta_i e^{-\psi_{i,2}} & \\
0 & & & \ddots
\end{bmatrix}
\begin{matrix} \\ \mathtt{I} \\ \\ \mathtt{J} \\ \end{matrix}
\end{array},
$$

where $\Delta_i := 1 + \overline{A}_i^{K^1_{e_i}} s_i^{K^1_{e_i}} \alpha_i e^{-\psi_{i,1}} + \overline{A}_i^{K^2_{e_i}} s_i^{K^2_{e_i}} \beta_i e^{-\psi_{i,2}}$. By construction, the nonzero entries of $\mathbf{T}^\rho_i$ are the contributions $\xi_i^{K_\mathtt{I}}$, $\xi_i^{K_\mathtt{J}}$ to the diagonal entries of $\mathbf{A}^\rho$ and the off-diagonal entries $A^\rho_{\mathtt{IJ}}$, $A^\rho_{\mathtt{JI}}$, from which we see that $\mathbf{T}^\rho_i$ is a nonsymmetric singular matrix with zero column sum. The global stiffness matrix $\mathbf{A}^\rho$ can therefore be partitioned into the sum of a symmetric positive definite part $\mathbf{A}^\rho_S$ (associated with

all the triangles belonging to the interior of Ω_1 and Ω_2) and of a non-symmetric part $\mathbf{A}^{\rho}_{NS} = \sum_{e_i \in \Gamma_m} \mathbf{T}^{\rho}_i$. By suitably renumbering the mesh elements, we see that the non-zero portion of matrix $\mathbf{A}^{\rho}_{NS}$ has a block diagonal structure, where each block of 2×2 size corresponds to the triangle pair sharing an edge on Γ_m (for example, $K_{\mathtt{I}}$, $K_{\mathtt{J}}$ or $K_{\mathtt{P}}$, $K_{\mathtt{Q}}$ in Fig.3).

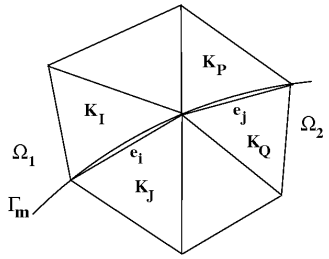

Figure 3. Neighbouring triangles across the menbrane.

Having characterized the structure and basic properties of the stiffness matrix $\mathbf{A}^{\rho}$, let us now investigate the numerical stability of the DMH-FV scheme. In this respect, an important issue in heterogeneous flow transport problems is that the adopted numerical scheme is *monotone* or, equivalently, it satisfies a *Discrete Maximum Principle* (DMP). This property is the discrete counterpart of the continuous maximum principle associated with problem (4), and is quite desirable because it prevents ρ_h from being affected by spurious oscillations and ensures that each component of $\boldsymbol{\rho}$ is positive if each component of the load vector $\mathbf{f}$ is > 0.

The need of devising a monotone approximation of problem (4) (typically studied under more standard Dirichlet-Neumann boundary conditions, i.e., without the presence of an internal interface) has driven a considerable interest towards the development of a special class of finite element schemes, known as exponentially fitted schemes (see [55] for a detailed analysis and references). Such schemes are based on the so–called Scharfetter–Gummel (SG) finite difference scheme [58], also known as Allen–Southwell method [29]. The SG method is an optimal upwind difference scheme, it is nodally exact in the case of constant problem coefficients [21] and satisfies a DMP irrespective of the relative weight between diffusive and convective terms. Extending the SG scheme to the two and three–dimensional setting, on triangular and tetrahedral decompositions of the computational domain, has been the object of several works: mixed-hybrid formulations [17,19,18,57], Petrov–Galerkin formulations [47,46,48,41], and Galerkin formulations with averaging of the model coefficients along the element edges [7,33,8,62,42]. These methods share some common features: (*i*) they recover the SG approximation if applied to one-dimensional problems; (*ii*) they satisfy a DMP under proper assumptions on the angles of the triangulation $\mathcal{T}_h$; (*iii*) they ensure flux conservation across suitably defined control volumes. Moreover, as a general trend, the schemes exhibit a common ability in capturing sharp fronts without spurious oscillations, at the price of introducing a certain amount of crosswind dissipation if the grid is not favorably aligned with the advection field (cf. the numerical experiments in [18,57] and [33]).

Moreover, in some cases (as in the mixed formulation proposed in [19,18]), the presence of a reaction term in the differential model introduces a difficulty in proving the DMP for any value of the coefficient and of the mesh size, and requires a suitable modification of the finite element space to reinforce the desired property [44]. Conceptually similar approaches (based on the use of a proper lumping quadrature formula) are adopted in the case of nodal-based formulations [10,9,41]

The following result provides sufficient conditions for the DMH-FV method to satisfy a DMP.

Proposition 3.1 *Let $\mathcal{T}_h$ be a Delaunay triangulation such that for each edge $e \in \Gamma_m$ we have $\theta_e^{K_e^1} \leq \pi/2$, $\theta_e^{K_e^2} \leq \pi/2$, and for each edge $e \in \Gamma_D \cup \Gamma_R$ we have $\theta_e^{K_e} \leq \pi/2$. Then, $\mathbf{A}^\rho$ is an irreducible M-matrix with strictly positive inverse [61], so that $\boldsymbol{\rho} > \mathbf{0}$ if $\mathbf{f} \geq \mathbf{0}$ (DMP).*

Proof 3.1 *Under the above geometric assumptions on $\mathcal{T}_h$ and the properties of $\mathbf{A}_S^\rho$ and $\mathbf{A}_{NS}^\rho$, it turns out that the stiffness matrix $\mathbf{A}^\rho$ has zero column sums, with strictly positive diagonal entries and nonpositive off diagonal entries. Moreover, for each element K with an edge on Γ_D, the matrix is diagonally dominant on the column corresponding to K. The result then immediately follows by application of Theorem 3.1, p.202 of [55].*

Prop. 3.1 provides a characterization of the numerical stability of the DMH-FV scheme under proper assumptions on the geometrical discretization. It is important to notice that the monotonicity of the proposed numerical method does not depend on the value of the reaction coefficient $ce^{-\psi}$ in (4), as is the case with the standard dual-mixed method of [19,18], because in the FV structure of the scheme such a term introduces a diagonal non-negative contribution to the stiffness matrix which increases its diagonal dominance. The requirement of weak acuteness of $\mathcal{T}_h$ on the domain external boundary is standard and not restrictive for implementation (see [62] and the references cited therein). The requirement of weak acuteness of $\mathcal{T}_h$ along the internal interface is not strictly necessary, as a sufficient (more general) condition for Prop. 3.1 to hold is that $\Delta_i > 0$ for each edge $e_i \in \Gamma_m$. In all the numerical experiments reported in Sect. 5 the finite element triangulation is chosen to be weakly acute along Γ_m and $\Gamma_D \cup \Gamma_R$.

The second remark concerns the relation between the proposed DMH-FV method and other classical methods for the numerical solution of (4). Each row of (23) is the finite volume discretization of the restriction to each element $K \in \mathcal{T}_h$ of the mass balance equation system $(4)_{1,2}$. Using Euler's theorem, we have that $\mathtt{Ne} \rightarrow 3\mathtt{NE}/2$ as the mesh size is refined, so that we can conclude that the computational effort of the DMH-FV method is substantially lower than that of the standard DMH formulation. Comparing the DMH-FV scheme to standard displacement-based methods, we see from relations (20) and (21) that in the former approach *both* Dirichlet and Robin boundary conditions are accounted for in an essential manner, unlike in the latter

where Robin conditions are accounted for in a weak manner. This indicates the robustness of the DMH-FV method in treating boundary conditions on the flux variable, which are typically the most important in the applications we are focusing on in the present article.

4 Implementation and Post-Processing of the DMH-FV Method

In this section, we discuss how to implement the DMH-FV method in a numerically stable manner and how to use the computed discrete solution to obtain a further approximation of the exact solution u of (1) that enjoys a better convergence behavior.

4.1 Implementation

The solution of system (23) is not convenient from the numerical standpoint because of the dynamic range of the function $e^{-\psi}$. This requires one to go back to the original variable u using the inverse of (3) on each element $K \in \mathcal{T}_h$ (cf. [19,18,16])

$$\rho^K = u^K \, e^{\psi^K} \qquad \forall K \in \mathcal{T}_h. \tag{27}$$

The action of (27) is a right diagonal scaling of $\mathbf{A}^\rho$ which transforms (23) into the equivalent algebraic linear system

$$\mathbf{A}^u \, \boldsymbol{u} = \mathbf{f}, \tag{28}$$

where $\mathbf{A}^u = \mathbf{A}^\rho \mathbf{D}^\psi \in \mathbb{R}^{\mathtt{NE}\times\mathtt{NE}}$ is the new stiffness matrix and $\boldsymbol{u} \in \mathbb{R}^{\mathtt{NE}}$ is the new unknown vector, $\mathbf{D}^\psi$ being a diagonal matrix such that $\mathbf{D}^\psi_{\mathtt{I}_K\mathtt{I}_K} = e^{\psi^K}$, $K \in \mathcal{T}_h$.

Proposition 4.1 *Under the same assumptions as in Prop. 3.1, we have that* $\mathbf{A}^u$ *is an M-matrix with strictly positive inverse. This implies that* $\boldsymbol{u} > \mathbf{0}$ *if* $\mathbf{f} \geq \mathbf{0}$.

4.2 Post-Processing

The approximate flux density $\boldsymbol{J}_h$ can be recovered from the computed solution of (28) by using (6) over each element $K \in \mathcal{T}_h$. With this aim, we need the expression of the flux Φ_i^K across each edge $\boldsymbol{e}_i \in \partial K$, $i = 1, 2, 3$, such that $\boldsymbol{e}_i \in \mathcal{E}_{h,int}$. A similar treatment holds for the edges belonging to Γ_D, Γ_R or Γ_m. Using (27) and (18) in (19) yields

$$\Phi_i^K = -\frac{e^{\Delta\psi_i^{K_i}} \, u^{K_i} - e^{\Delta\psi_i^K} \, u^K}{\zeta_i^K + \zeta_i^{K_i}} |\boldsymbol{e}_i| \qquad \boldsymbol{e}_i \in \partial K \cap \mathcal{E}_{h,int}. \tag{29}$$

Proposition 4.2 *Let $\boldsymbol{e}_i \in \partial K \cap \mathcal{E}_{h,int}$ and assume that $D^K = D^{K_i} \equiv D$ and that $\psi \in C^1([C_K, C_{K_i}])$. Then, the flux approximation* (29) *coincides with the classical Scharfetter-Gummel (SG) exponentially fitted difference formula [58]*

$$\Phi_i^K = -D\,\frac{u^{K_i}\,Be(\Delta\psi_i) - u^K\,Be(-\Delta\psi_i)}{s_i}|\boldsymbol{e}_i|, \qquad \Delta\psi_i := \psi^K - \psi^{K_i}. \tag{30}$$

Proof 4.1 *We have to prove that:*

$$\begin{aligned} \frac{e^{\Delta\psi_i^K}}{\dfrac{s_i^K}{Be(\Delta\psi_i^1)} + \dfrac{s_i^{K_i}}{Be(\Delta\psi_i^2)}} &= \frac{Be(-\Delta\psi_i)}{s_i} \\ \frac{e^{\Delta\psi_i^{K_i}}}{\dfrac{s_i^{K_i}}{Be(\Delta\psi_i^1)} + \dfrac{s_i^{K_i}}{Be(\Delta\psi_i^2)}} &= \frac{Be(\Delta\psi_i)}{s_i}. \end{aligned} \tag{31}$$

Let us consider $(31)_1$. *Noting that $\Delta\psi_i = \Delta\psi_i^K - \Delta\psi_i^{K_i}$, we have*

$$\frac{Be(-\Delta\psi_i)}{s_i} = \frac{-\Delta\psi_i}{s_i(e^{-\Delta\psi_i}-1)} = \frac{-\Delta\psi_i\,e^{\Delta\psi_i^K}}{s_i(e^{\Delta\psi_i^{K_i}} - e^{\Delta\psi_i^K})} = \frac{e^{\Delta\psi_i^K}}{\dfrac{e^{\Delta\psi_i^K}-1}{\Delta\psi_i/s_i} - \dfrac{e^{\Delta\psi_i^{K_i}}-1}{\Delta\psi_i/s_i}},$$

which coincides with the left-hand side of $(31)_1$ *because $\Delta\psi_i^K = \Delta\psi_i(s_i^K/s_i)$ and $\Delta\psi_i^{K_i} = -\Delta\psi_i(s_i^{K_i}/s_i)$. In the same manner, we prove* $(31)_2$.

Proposition 4.2 shows that (29) is the consistent generalization of the SG method to the case where *both* diffusivity coefficient and advective field are piecewise constant quantities over the interval s_e, with a possible finite jump discontinuity in correspondance of the midpoint M_e of the inter-element edge $\mathbf{e}$. This connection between the DMH-FV formulation and the SG discretization is relevant in view of the analysis of the numerical performance of the former scheme in the presence of dominating convection, as thoroughly addressed in Sect.5.

Let $\widehat{\lambda}_h \in \Lambda_h$ be the hybrid variable representing the approximation of u over $\mathcal{E}_h$. To recover $\widehat{\lambda}_h$ from the computed solution of (28) we need to use (17) and then apply (18), (8), (27) and (3) to obtain

$$\widehat{\lambda}_e = \frac{\zeta_e^2\,e^{\Delta\psi^{K_e^1}}\,u^{K_e^1} + \zeta_e^1\,e^{\Delta\psi^{K_e^2}}\,u^{K_e^2}}{\zeta_e^1 + \zeta_e^2} \qquad \forall \boldsymbol{e} \in \mathcal{E}_{h,int}. \tag{32}$$

A similar treatment holds for the edges belonging to Γ_D, Γ_R and Γ_m, to yield:

$$\widehat{\lambda}_e = \begin{cases} \mathcal{P}_0(u_{D,e}) & \boldsymbol{e} \in \Gamma_D \\ \dfrac{e^{\Delta\psi^K}\,u^K - \zeta_e\,j_{Re}}{1+\gamma_e\,\zeta_e^K} & \boldsymbol{e} \in \Gamma_R, \end{cases} \tag{33}$$

while on Γ_m we have:

$$\widehat{\lambda}_{e,1} = \frac{e^{\Delta\psi^{K_e^1}}\ (1+\beta_e\,\zeta_e^2)\ u^{K_e^1} + \beta_e\,\zeta_e^1\,e^{\Delta\psi^{K_e^2}}\,u^{K_e^2} - \zeta_e^1\,(\sigma_{e,1} + \ \beta_e\,\zeta_e^2\,(\sigma_{e,1} - \sigma_{e,2}))}{1+\alpha_e\,\zeta_e^1+\beta_e\,\zeta_e^2}$$

$$\widehat{\lambda}_{e,2} = \frac{e^{\Delta\psi^{K_e^2}}\ (1+\alpha_e\,\zeta_e^1)\ u^{K_e^2} + \alpha_e\,\zeta_e^2\,e^{\Delta\psi^{K_e^1}}\,u^{K_e^1} + \zeta_e^2\,(\sigma_{e,2} + \ \alpha_e\,\zeta_e^1\,(\sigma_{e,2} - \sigma_{e,1}))}{1+\alpha_e\,\zeta_e^1+\beta_e\,\zeta_e^2}. \tag{34}$$

The above expressions of the degrees of freedom of $\widehat{\lambda}_h$ over $\mathcal{E}_h$ can be used to construct the following approximation of the exact solution u of (1)

$$u_h^*(\boldsymbol{x}) = \sum_{e\in\mathcal{E}_h} \widehat{\lambda}_e\ \omega_e(\boldsymbol{x}), \qquad \boldsymbol{x}\in\Omega. \tag{35}$$

The function $u_h^* \in \Lambda_h$ is the non-conforming piecewise linear interpolate of $\widehat{\lambda}_h$ over the computational grid $\mathcal{T}_h$. A thorough experimental analysis illustrated in Sect.5 demonstrates that u_h^* satisfies the following convergence result

$$\|u - u_h^*\|_{L^2(\Omega)} \leq Ch^2, \tag{36}$$

C being a positive constant depending on u and $\boldsymbol{J}$ but independent of the mesh size h. Since the expected order of accuracy of u_h in the L^2-norm is $\mathcal{O}(h)$, we conclude that (36) represents the *superconvergence* of the non-conforming approximation u_h^* to the exact solution u of (1), indicating, at least experimentally, that the DMH-FV method, applied to the heterogeneous transport model, enjoys the same convergence behavior proved in [4] for the standard DMH formulation in the case of the elliptic model problem with Dirichlet boundary conditions. The steps to prove (36) can be sketched as follows. Assume that the exact solution $(\boldsymbol{J},\rho)$ of (4) satisfies suitable regularity properties and that $\mathcal{T}_h$, α, β and ψ are as in Theorem 3.1. Then:

i) using (10) and the analysis of Refs. [45,16], we can show that the solution triple $(\boldsymbol{J}_h,\rho_h,\lambda_h)$ of the DMH approximation with the numerical quadrature (7) satisfies the same optimal error estimates valid for the DMH method in the case of exact integration (see [4]);

ii) using Theorem 2.2 of [4] we obtain that the non-conforming piecewise linear interpolate ρ_h^* of λ_h over the computational grid $\mathcal{T}_h$ satisfies

$$\|\rho - \rho_h^*\|_{L^2(\Omega)} \leq Ch^2, \tag{37}$$

for a positive constant C depending on ρ and $\boldsymbol{J}$ but independent of h;

iii) using (3) and triangle inequality, we get

$$\|u - u_h^*\|_{L^2(\Omega)} \leq \|(\rho-\rho_h^*)e^{-\psi}\|_{L^2(\Omega)} + \|\rho_h^* e^{-\psi} - (\lambda_h e^{-\psi})^*\|_{L^2(\Omega)}.$$

The first term on the right-hand side can be bounded by using (37) while the second term can be bounded by using interpolation theory and the a-priori control on λ_h provided by the DMP. This concludes the sketch of the proof of (36).

5 Numerical Results

In this section, we perform a thorough numerical validation of the DMH-FV method in the study of three test problems which represent significant examples of realistic applications in Biology and Electrophysiology.

5.1 A One-Dimensional Heterogeneous Domain

In this section, we consider problem (1) in the case where $\Omega = (0,1) \times (-0.5, 0.5)$ and a membrane Γ_m is located at $x = 0.5$ to separate the left subdomain Ω_1 from the right subdomain Ω_2. We set $f = 0$ and $\boldsymbol{\nabla}\psi = [-5,\, 0]^T$, while having two different constant values in each subdomain for the diffusion constant $D_1 = 50$, $D_2 = 0.5$. The Dirichlet data are $u_D = 0$ at $x = 0, y \in [-0.5, 0.5]$ and $u_D = 1$ at $x = 1, y \in [-0.5, 0.5]$, while homogeneous Neumann conditions are enforced along $y = 0.5$ and $y = -0.5$, and $\sigma_1 = \sigma_2 = 0$ on the interface. These data correspond to a one-dimensional transmembrane flow along the x-direction. The following three sets of input data are considered: 1) $c_1 = c_2 = 0$ and $\alpha = \beta$ with $\alpha \to +\infty$; 2) $c_1 = c_2 = 0$ and $\alpha = \beta = 10$; 3) $c_1 = 0.1$, $c_2 = 10$ while again $\alpha = \beta = 10$. Notice that case 1) corresponds to enforcing that u and $\boldsymbol{J} \cdot \boldsymbol{n}$ are continuous across Γ_m. The computed solutions for cases 1) and 2) are depicted in Fig. 4 (left), representing a section at $y = 0$ of the post-processed quantity u_h^*. The problem is diffusion–dominated in Ω_1, and is advection-dominated in Ω_2, with an exact solution u almost linear over Ω_1 and exponential over Ω_2. In case 2), the solution has a finite jump across Γ_m because of the selective behaviour of the membrane, while in case 1), the solution is continuous, because the membrane is completely transparent to the flow of transported mass since the interface condition is reduced to $u_1 = u_2$ on Γ_m, which is equivalent to eliminating the membrane and treating the edges on Γ_m as belonging to $\mathcal{E}_{h,int}$. In any case, the DMH-FV method captures the solution layer without introducing spurious oscillations, and it can be checked that the post-processed solution u_h^* is nodally exact up to machine precision. In case 3), because of the fact that $c \neq 0$, the variable u_h^* is no longer nodally exact; however, the experimental convergence analysis reported in Fig.4 (right) indicates that u_h^* exhibits second order accuracy according to the error estimate (36). Fig. 5 shows a three-dimensional plot of u_h^*. The finite jump across Γ_m and the non-conforming interpolation properties of the finite element space Λ_h are clearly visible.

5.2 Stationary Profile of a Binary Electrolyte at a Boundary

In this section, we apply the DMH-FV to numerically study the Poisson-Nernst-Planck (PNP) system of partial differential equations describing the electro-diffusive

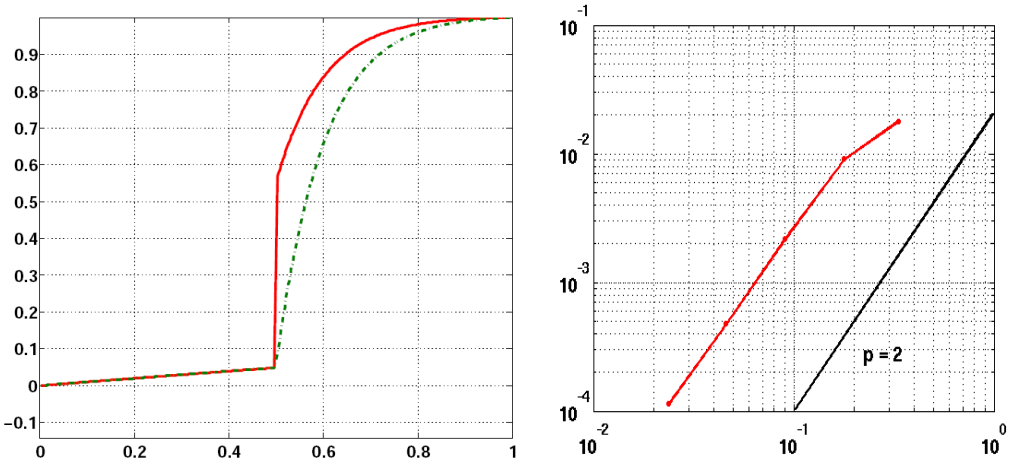

Figure 4. Left: u_h^*. Solid line: $\alpha = \beta = 10$, dash-dotted line: $\alpha = \beta \to \infty$. Right: $\|u - u_h^*\|_{L^2(\Omega)}$ as a function of the mesh size h.

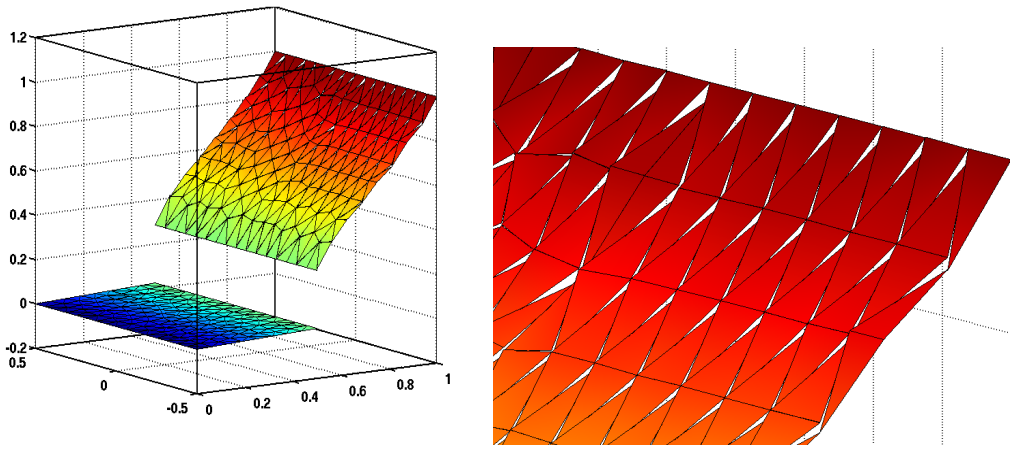

Figure 5. Left: post-processed solution u_h^* in the case $c_1 = 0.1$, $c_2 = 10$ and $\alpha = \beta = 10$. Right: zoom of the solution on Ω_2.

transport of M ionic species u_i, $i = 1, \ldots, M$, with valence z_i, throughout an electrolyte medium [56]:

$$\begin{cases} \text{div}\, \boldsymbol{J_i} + q\, z_i \dfrac{\partial c_i}{\partial t} = 0 & i = 1 \ldots M \\ \text{div}\, \boldsymbol{D} = q \sum_{i=1}^{M} z_i\, c_i + \rho_0 & \\ \boldsymbol{J_i} = -q z_i\, D_i \left(\boldsymbol{\nabla} c_i + \dfrac{q z_i c_i}{k_B T} \boldsymbol{\nabla} \psi \right) & i = 1 \ldots M \\ \boldsymbol{D} = \varepsilon_w\, \boldsymbol{E} = -\varepsilon_w\, \boldsymbol{\nabla} \psi. & \end{cases} \tag{38}$$

The dependent variables of the system are the concentrations c_i of the i-th ionic species (e.g. Na^+, K^+, Cl^-), while the ionic current densities $\boldsymbol{J_i}$ and the polarization vector $\boldsymbol{D}$ are related to the potential ψ by the Poisson equation $(38)_4$. D_i is the diffusion coefficient in an aqueous medium for the i-th species of ion, k_B is

the Boltzmann constant, T is the absolute temperature, q the elementary charge, z_i the valence of each ion, ε_w the dielectric constant of water and ρ_0 the fixed charge density, assumed to be equal to zero as there are no fixed charge in the intra- or extracellular space. The diffusion coefficients are related to the mobility coefficient by the well-known Einstein relation, that is $D_i = \frac{k_B T}{q|z_i|}\,\mu_i$, where μ_i is the electrical mobility of the i-th ion in water.

In the stationary case ($\partial c_i/\partial t = 0$), the PNP nonlinear differential system is treated using a decoupled functional iteration similar to the classical Gummel's map [36] widely employed in semiconductor device simulation (for the details of the algorithm and its computer implementation, we refer to [12]). This leads to the successive solution of linearized differential subproblems of the form (1). In the considered case, we have a binary electrolyte (i.e., $M = 2$) with $z_i = \pm 1$, and the boundary value problem (38) is to be solved in the semi-infinite domain $x \in [0, +\infty)$ with an applied external voltage drop $\Delta V_{ext} = \psi(0) - \psi(+\infty) = 100mV$, with $\psi(+\infty) = 0$ and a surface at $x = 0$ impermeable to the ions. An analytical solution of this problem for ψ and $u_{1,2}$ can be written as [13]:

$$\psi = 2\,V_T\,\log\left(\frac{1 + K\exp(-\sqrt{2}\,x/L_D)}{1 - K\exp(-\sqrt{2}\,x/L_D)}\right)$$
$$u_i = N_0\,\exp\left(-q\,z_i\,\psi/V_T\right),$$

where $K = \tanh(\Delta V_{ext}/V_T)$, $L_D = \sqrt{\varepsilon\,V_T/(q\,N_0)}$ is the Debye length, $V_T \approx 25\,mV$ is the thermal voltage (having assumed $T = 300\,K$), q is the unit charge, $\varepsilon \approx 7 \cdot 10^{-10}\,Fm^{-1}$ is the dielectric constant of the medium (water in this case) and $N_0 = 1\,mM$ is the bulk concentration of both ions. The performed simulation is actually carried out on the two-dimensional domain $\Omega = (0, L)^2$, with $L = 5\,L_D$. The Debye length gives a measure of the screening effect of a space charge layer, so that the choice of truncating the semi-infinite domain to a finite length equal to a positive multiple of L_D is a very good approximation of the decaying behavior of ionic densities far away from the layer. The boundary conditions for ψ and $u_{1,2}$ on $y = 0$ and $y = 5\,L_D$ are of homogeneous Neumann type in order to obtain a solution dependent upon x solely, while on $x = 0$ and $x = 5\,L_D$ the boundary conditions are obtained from the analytical solution. Fig. 6 illustrates a slice along the x-axis of the computed ion concentrations c_i and the discretization error as a function of h. No spurious oscillations affect the results, and, again, superconvergence as predicted by (36) can be observed for both u_1 and u_2.

5.3 Simulation of a Neuro-Chip

In this concluding section, we carry out a validation of the numerical accuracy and robustness of the DMH-FV formulation in the simulation, using the PNP differential model, of a basic configuration of a neuro-chip for neuroscience applications

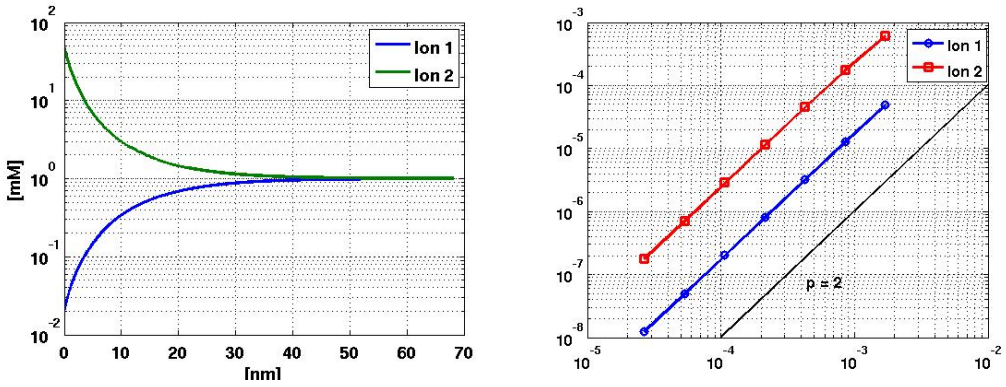

Figure 6. Computed ion concentrations (left) and $\|u_i - u_{i,h}^*\|_{L^2(\Omega)}$, $i = 1, 2$ (right).

[63,59,32,20]. The bio-hybrid device considered in this section is the EOSFET (Electrolyte Oxide-Semiconductor Field Effect Transistor) schematically depicted in Fig. 7 (left). The aim of the device is to interface a biological component (a neuronal cell) to an electrical component (solid-state substrate), in order (*i*) to transduce a chemical signal generated by the biological component into an electronically readable signal, or, viceversa, (*ii*) to activate the biological component by the application of an electronic signal. In operation mode (*i*), the EOSFET is working as a bio-sensor, while in operation mode (*ii*) the EOSFET is working as a neuro-prosthetic device, i.e., playing the role of a neuronal connection or even of a full neuronal network, thus opening the view for future use of the neuro-chip as a cure for neuro-degenerative deseases like Alzheimer or Parkinson [6]. The

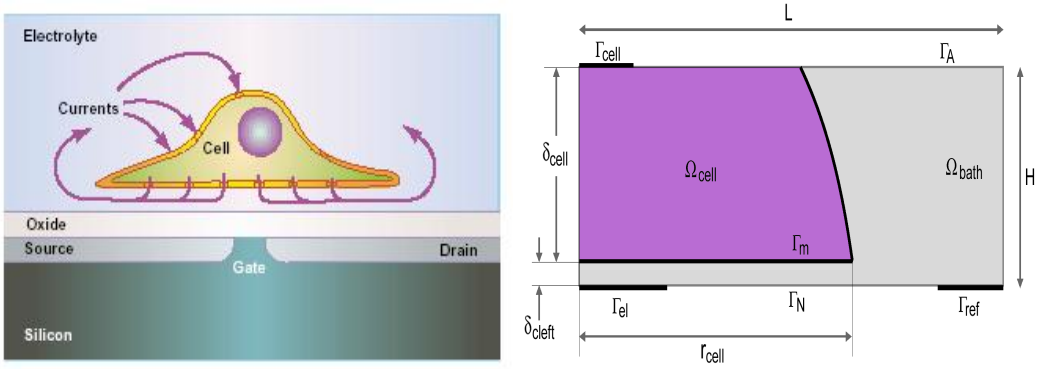

Figure 7. Left: schematics of a neuro-chip (by courtesy reprinted from: E. Neher, Molecular biology meets microelectronics, Nature Biotechnology, **19**, 114 (2001)). Right: computational domain for stationary neuro-chip simulation.

computational domain Ω is depicted in Fig. 7 (right), where we can distinguish a portion Ω_{cell} of the cell cytoplasm, the interstitial electrolyte cleft Ω_{bath} separating cell from substrate, the cell membrane Γ_m, the cell-to-chip contacting interface Γ_{el} and two reference contacts Γ_{cell} and Γ_{ref}. Dirichlet boundary conditions as in $(1)_3$ are enforced on Γ_{cell} and Γ_{ref}, a Robin boundary condition as in $(1)_4$ is enforced on Γ_{el}, while interface boundary conditions as in $(1)_{5,6}$ are enforced on Γ_m. On the remaining portions of the domain boundary, Γ_A, Γ_N and the left ver-

tical side of Ω, a homogeneous Neumann condition is enforced ($\gamma = j_R = 0$ in $(1)_4$). The geometrical data used in computations are $L = 0.8\,\mu m$, $H = 0.3\,\mu m$, $\delta_{cell} = 0.25, \mu m$, $r_{cell} = 0.5\,\mu m$ and $\delta_{cleft} = 50\,nm$. Ionic charge flow includes three species, K^+, Na^+ and Cl^-, whose reference values are kept fixed respectively at $(139, 12, 151)\,mM$ on Γ_{cell} and $(4, 145, 149)\,mM$ on Γ_{ref}. As for the boundary condition for the electrostatic potential ψ, we set $\psi = 0\,V$ on Γ_{ref} and $\psi \in [-100, +60]\,mV$ on Γ_{cell}. On the membrane Γ_m, interface conditions for the potential ψ are enforced in order to model a distributed fixed capacitance, while the Goldman-Hodgkin-Katz model [40] is used to describe the flow of ionic concentrations through the membrane:

$$\begin{cases} -\varepsilon \boldsymbol{\nabla}\psi \cdot \boldsymbol{n}_{\Gamma_m} = C_m \left(\psi^{int} - \psi^{ext}\right), \\ \boldsymbol{J_i} \cdot \boldsymbol{n}_{\Gamma_m} = P_i\, q\, z_i \left(Be\left(\dfrac{-z_i\,\psi_m}{V_T}\right) n_i^{int} - Be\left(\dfrac{z_i\,\psi_m}{V_T}\right) n_i^{ext} \right) \;\forall\, i, \end{cases}$$

where ^{int}, ^{ext} refer to the interior and exterior sides of the membrane, C_m is the capacitance per unit area of the membrane, $\psi_m = \psi^{int} - \psi^{ext}$ and P_i is the permeability for the specific i-th ion. On Γ_{el}, an homogeneous Neumann condition is enforced for the concentrations c_i, while the following compatibility condition is enforced for the polarization vector $\boldsymbol{D}$

$$-\varepsilon_w \boldsymbol{\nabla}\psi \cdot \boldsymbol{n}_{\Gamma_{el}} = C_{el}(\psi)\left(\psi - V_{el}\right),$$

where V_{el} is a fixed external potential and $C_{el}(\psi)$ is a MOS (Metal Oxide Semiconductor) capacitance nonlinearly depending upon ψ as described, e.g., in [60].

Fig. 8 (left) shows the computed static current-voltage characteristics, which describes the behaviour of the average value of $\mathbf{J}_i \cdot \mathbf{n}|_{\Gamma_{ref}}$ (positive if current flows out of Γ_{ref}, negative otherwise) as a function of $\psi|_{\Gamma_{cell}}$. The accuracy of the results is demonstrated by the very good agreement of the estimated reverse potential $V_{rev,i} = V_T \,/\, z_i \,\log(n_i^{ext} / \, n_i^{int})$ of each ionic species, that is the value of $\psi|_{\Gamma_{cell}}$ at which the ionic current density is equal to zero, with typical data in electrophysiology measurements [40,34]. Fig. 8 (right) shows the distribution of potassium current density over the computational domain. We can notice the higher current density in the cleft region between the cell membrane and the electrical substrate. Such higher current density in turn causes the rise of the potential in the cleft region, which can be measured by the field-effect transistor in the substrate. Computed current value is again in quite a good agreement with measured data [20]. We conclude this discussion by showing in Fig. 9 the computed variations over $\mathcal{T}_h$ of the electric potential ψ and of the Na^+ concentration with respect to their corrsponding reference values (enforced at the Dirichlet boundary). The results give an idea of the steep boundary layer effects occurring across the membrane separating the intracellular region from the electrolyte cleft and at the interface with the electronic substrate, and demonstrates the effectiveness of the DMH-FV formulation in capturing the essential phenomena without introducing spurious oscillations that would

otherwise make the simulation prediction completely unreliable and inaccurate.

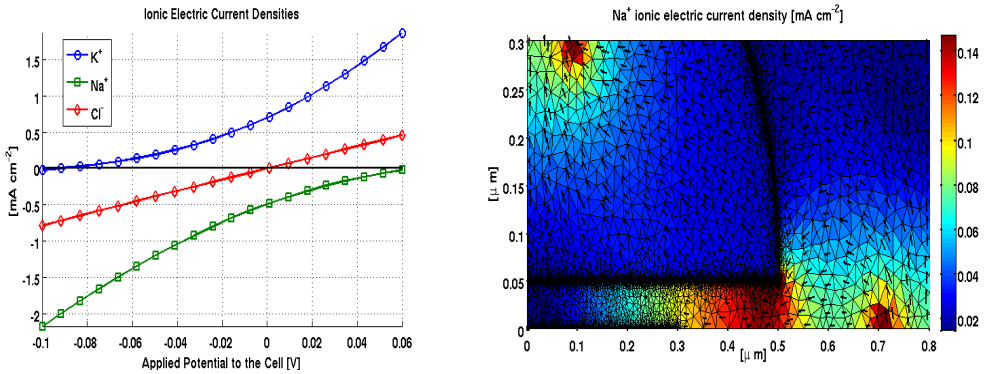

Figure 8. Left: static current–voltage characteristics. Right: computed Na^+ current density.

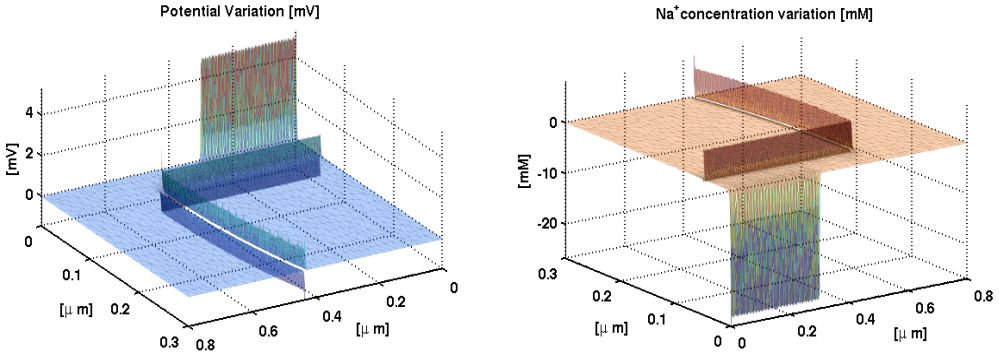

Figure 9. Variations with respect to reference values of potential (left) and Na^+ concentration (right).

6 Conclusions

In this article, we have proposed, analyzed and numerically validated a novel dual mixed-hybridized finite volume (DMH-FV) method for the discretization of transport problems in heterogeneous domains separated by a membrane.

The DMH-FV scheme has the same mathematical structure as standard DMH formulations, and enjoys their convergence and conservation properties.

An attractive extra feature of the proposed new method is that it can be implemented as a genuine finite volume scheme with a considerable benefit in terms of computational saving compared to the classical DMH approach.

Moreover, another relevant property of the FV variant of the DMH method is that, under mild assumptions on the computational grid, it satisfies a discrete maximum principle, which ensures that the computed solution is strictly positive if the right-hand side of the linear algebraic system is so. This property is quite desirable in the

application at hand where, typically, the primal variable of the model is a concentration.

The novel DMH-FV scheme has proved to be accurate and robust in all of the perfomed numerical experiments. This is very promising for future use of the scheme in the simulation of complex problems in Computational Biology and Neuroscience. To give an idea of the potentiality of the method in these applications, we show in Fig. 10 two time snapshots of the simulation of the action potential propagation along an unmyelinated neuronal axon, as originally considered in [35] and numerically investigated in [50]. Results clearly reproduce the spreading of the action potential towards the two ends of the axon without introducing spurious oscillations, while accounting for the finite potential jump occurring across the membrane.

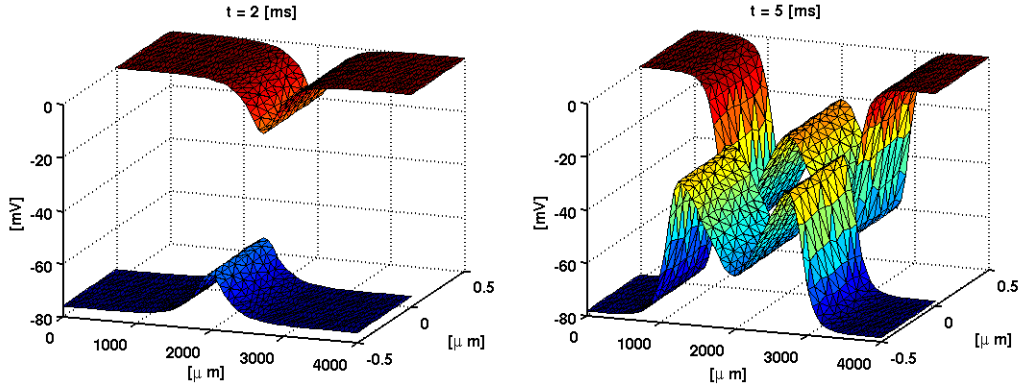

Figure 10. Computed action potential at two different time levels.

Acknowledgements

The first author availed himself of the computer and environmental facilities provided by the Dipartimento di Matematica "F. Brioschi", Politecnico di Milano. The second author was supported by ONR/Darpa grant nr. LLCN00014-05-C-0241. The third author was supported by NSF-DMS grant no. 0914963 as well as the Alfred P. Sloan foundation. The fourth author was partly supported by the MIUR grant nr. 2006013187-003.

References

[1] In C.P. Fall, E.S. Marland, J.M. Wagner, and J.J. Tyson, editors, *Computational Cell Biology*, volume 20 of *Interdisciplinary Applied Mathematics*. Springer, New York, 2002. 1st ed 2002. Corr. 3rd printing, 2004.

[2] In G.E. Karniadakis, A. Beskok, and N. Aluru, editors, *Microflows and Nanoflows. Fundamentals and Simulation*, volume 29 of *Interdisciplinary Applied Mathematics*. Springer, New York, 2005.

[3] A. Agouzal, J. Baranger, J.F. Maitre, and F. Oudin. Connection between finite volume and mixed finite element methods for a diffusion problem with nonconstant coefficients. application to a convection-diffusion problem. *East-West J. Numer. Math.*, 34:237–254, 1995.

[4] D.N. Arnold and F. Brezzi. Mixed and Nonconforming Finite Element Methods: Implementation, Postprocessing and Error Estimates. *Math. Modeling and Numer. Anal.*, 19-1:7–32, 1985.

[5] I. Babuska and J. Osborn. Generalized finite element methods, their performance and their relation to mixed methods. *SIAM J. Numer. Anal.*, 20:510–536, 1983.

[6] M. Bani-Yaghoub, R. Tremblay, R. Voicu, G. Mealing, R. Monette, C. Py, K. Faid, and M. Sikorska. Neurogenesis and neuronal communication on micropatterned neurochips. *Biotechnology and Bioengineering*, 92 (3):336–345, 2005.

[7] R.E. Bank, J.F. Burgler, W. Fichtner, and R.K. Smith. Some upwinding techniques for finite element approximations of convection-diffusion equations. *Numer. Math.*, 58:185–202, 1990.

[8] R.E. Bank, W.M. Coughran Jr., and L.C. Cowsar. The finite volume Scharfetter–Gummel method for steady convection–diffusion equations. *Comput. Visual. Sci.*, 1(3):123–136, 1998.

[9] R.E. Bank and D.J. Rose. Some error estimates for the box method. *SIAM J. Numer. Anal.*, 24(4):777–787, 1987.

[10] R.E. Bank, D.J. Rose, and W. Fichtner. Numerical methods for semiconductor device simulation. *SIAM J. Sci. and Stat. Comput.*, 4:416–435, 1983.

[11] J. Baranger, J.F. Maitre, and F. Oudin. Connection between finite volume and mixed finite element methods. M^2AN, 30:445–465, 1996.

[12] M. Brera. Multiphysics/multiscale computational modeling in neuroelectronics, 2009. Master Thesis, Politecnico di Milano, `http://www1.mate.polimi.it/biblioteca/tesvview.php?id=66&L=i`.

[13] C.M.A. Brett and A.M. Oliveira Brett. *Electrochemistry: Principles, Methods, and Applications*. Oxford University Press, USA, 7 1993.

[14] F. Brezzi and M. Fortin. *Mixed and Hybrid Finite Element Methods*. Springer Verlag, New York, 1991.

[15] F. Brezzi, L.D. Marini, S. Micheletti, P. Pietra, and R. Sacco. Stability and error analysis of mixed finite volume methods for advective-diffusive problems. *Comput. Math. Appl.*, 51:681–696, 2006.

[16] F. Brezzi, L.D. Marini, S. Micheletti, P. Pietra, R. Sacco, and S. Wang. Discretization of semiconductor device problems (i). In E.J.W. ter Maten P.G. Ciarlet, W.H.A. Schilders, editor, *Lecture Notes in Computational Science and Engineering*, volume XIII, pages 317–441. Elsevier North-Holland, Amsterdam, 2005.

[17] F. Brezzi, L.D. Marini, and P. Pietra. Méthodes d'éléments finis mixtes et schéma de Scharfetter–Gummel. *C.R. Acad. Sci. Paris*, 305, Série 1:599–604, 1987.

[18] F. Brezzi, L.D. Marini, and P. Pietra. Numerical simulation of semiconductor devices. *Comput. Meths. Appl. Mech. and Engr.*, 75:493–514, 1989.

[19] F. Brezzi, L.D. Marini, and P. Pietra. Two-dimensional exponential fitting and applications to drift-diffusion models. *SIAM J. Numer. Anal.*, 26:1342–1355, 1989.

[20] M. Brittinger and P. Fromherz. Field-effect transistor with recombinant potassium channels: fast and slow response by electrical and chemical interactions. *Appl. Phys. A*, 81:439–447, 2005.

[21] A.N. Brooks and T.J.R. Hughes. Streamline upwind Petrov-Galerkin formulations for convection dominated flows with particular emphasis on the incompressible Navier-Stokes equations. *Comput. Meths. Appl. Mech. and Engr.*, 32:199–259, 1982.

[22] B. Cockburn, B. Dong, and J. Guzmán. A superconvergent LDG-hybridizable Galerkin method for second-order elliptic problems. *Math. Comp.*, 77:1887–1916, 2008.

[23] B. Cockburn, B. Dong, J. Guzman, M. Restelli, and R. Sacco. An hybridizable discontinuous galerkin method for steady-state convection-diffusion-reaction problems. *SIAM J. Sci. Comp.*, 31 (5):3827–3846, 2009.

[24] B. Cockburn and J. Gopalakrishnan. A characterization of hybridized mixed methods for second order elliptic problems. *SIAM J. Numer. Anal.*, 42:283–301, 2004.

[25] B. Cockburn and J. Gopalakrishnan. Error analysis of variable degree mixed methods for elliptic problems via hybridization. *Math. Comp.*, 74:1653–1677, 2005.

[26] B. Cockburn, J. Gopalakrishnan, and R. Lazarov. Unified hybridization of discontinuous Galerkin, mixed and continuous Galerkin methods for second order elliptic problems. *SIAM J. Numer. Anal.*, 47:1319–1365, 2009.

[27] B. Cockburn, J. Guzmán, and H. Wang. Superconvergent discontinuous Galerkin methods for second-order elliptic problems. *Math. Comp.*, 78:1–24, 2009.

[28] M. Crouzeix and P.A. Raviart. Conforming and non-conforming finite element methods for solving the stationary Stokes equations. *R.A.I.R.O.*, R-3:33–76, 1973.

[29] D.N. de G. Allen and R.V. Southwell. Relaxation methods applied to determine the motion, in two dimensions, of a viscous fluid past a fixed cylinder. *Quart. J. Mech. Appl. Math.*, 8:129–145, 1955.

[30] B. Delaunay. Sur la sphère vide. *Izv. Akad. Nauk. SSSR., Math. and Nat. Sci. Div.*, 6:793–800, 1934.

[31] P.J. Frey and P.-L. George. *Mesh Generation. Application to Finite Elements (2nd Ed.)*. Wiley, London, 2008.

[32] P. Fromherz. Neuroelectronics interfacing: Semiconductor chips with ion channels, nerve cells and brain. In R. Weise, editor, *Nanoelectronics and Information Technology*, pages 781–810. Wiley-VCH, Berlin, 2003.

[33] E. Gatti, S. Micheletti, and R. Sacco. A new Galerkin framework for the drift-diffusion equation in semiconductors. *East-West J. Numer. Math.*, 6(2):101–135, 1998.

[34] B. Hille. *Ionic Channels of Excitable Membranes*. Sinauer Associates, Inc., Sunderland, MA, 2001.

[35] A.L. Hodgkin and A.F. Huxley. Currents carried by sodium and potassium ions through the membrane of the giant axon of *loligo*. *Journal of Physiology*, 116:449–472, 1952.

[36] J.W. Jerome. *Analysis of Charge Transport*. Springer-Verlag, Berlin Heidelberg, 1996.

[37] J.W. Jerome. Analytical approaches to charge transport in a moving medium. *Transport Theory and Statistical Physics*, 31:333–366, 2002.

[38] J.W. Jerome and R. Sacco. Global weak solutions for an incompressible charged fluid with multi-scale couplings: Initial-boundary value problem. *Nonlinear Analysis*, 71:e2487–e2497, 2009.

[39] J.W. Jerome, R. Sacco, B. Chini, and M. Longaretti. Computational modeling and simulation of complex systems in bio-electronics. *Journal of Computational Electronics*, **7** (1):10–13, 2008.

[40] J. Keener and J. Sneyd. *Mathematical Physiology*. Springer–Verlag, New York, 1998.

[41] T. Kerkhoven. Piecewise linear Petrov–Galerkin error estimates for the box method. *SIAM J. Numer. Anal.*, 33(5):1864–1884, 1996.

[42] R.D. Lazarov and L.T. Zikatanov. An exponential fitting scheme for general convection–diffusion equations on tetrahedral meshes. *Comput. Appl. Math., (Obchysljuval'na ta prykladna matematyka, Kiev)*, 1(92):60–69, 2005.

[43] M. Longaretti, G. Marino, B. Chini, J.W. Jerome, and R. Sacco. Computational modeling in nano-bio-electronics: simulation of ionic transport in voltage operated channels. *Journal of Journal of Nanoscience and Nanotechnology*, **8**:1–9, 2007.

[44] L.D. Marini and P. Pietra. An abstract theory for mixed approximations of second order elliptic problems. *Math. Aplic. Comp.*, 8:219–239, 1990.

[45] S. Micheletti, R. Sacco, and F. Saleri. On some mixed finite element methods with numerical integration. *SIAM J. Sci. Comput.*, 23-1:245–270, 2001.

[46] J.J. Miller and S. Wang. An analysis of the Scharfetter-Gummel box method for the stationary semiconductor device equations. *RAIRO M^2AN*, 28(2):123–140, 1994.

[47] J.J. Miller and S. Wang. A new non–conforming Petrov–Galerkin finite element method with triangular elements for an advection–diffusion problem. *IMA J. Numer. Anal.*, 14:257–276, 1994.

[48] J.J. Miller and S. Wang. A tetrahedral mixed finite element method for the stationary semiconductor continuity equations. *SIAM J. Numer. Anal.*, 31 (1):196–216, 1994.

[49] Y. Mori, J .W. Jerome, and C. S. Peskin. A three-dimensional model of cellular electrical activity. *Bulletin of the Institute of Mathematics, Academia Sinica*, 2 (2):367–390, 2007.

[50] Y. Mori and C. S. Peskin. A numerical method for cellular electrophysiology based on the electrodiffusion equations with internal boundary conditions at internal membranes. To appear in Communications in Applied Mathematics and Computational Science, 2009.

[51] A. Quarteroni and A. Valli. *Numerical Approximation of Partial Differential Equations*. Springer-Verlag, New York, Berlin, 1994.

[52] P.A. Raviart and J.M. Thomas. A mixed finite element method for second order elliptic problems. In I. Galligani and E. Magenes, editors, *Mathematical Aspects of Finite Element Methods,I*. Springer-Verlag, Berlin, 1977.

[53] P.A. Raviart and J.M. Thomas. Dual finite element methods for second order elliptic problems. In R. Glowinski, E.Y. Rodin, and O.C. Zienkiewicz, editors, *Energy methods in finite element analysis*. John Wiley and Sons Ltd., New-York, 1979.

[54] J.E. Roberts and J.M. Thomas. Mixed and hybrid methods. In P.G. Ciarlet and J.L. Lions, editors, *Finite Element Methods, Part I*. North-Holland, Amsterdam, 1991. Vol.2.

[55] H. G. Roos, M. Stynes, and L. Tobiska. *Numerical methods for singularly perturbed differential equations*. Springer-Verlag, Berlin Heidelberg, 1996.

[56] I. Rubinstein. *Electrodiffusion of Ions*. SIAM, Philadelphia, PA, 1990.

[57] R. Sacco and F. Saleri. Stabilized mixed finite volume methods for convection-diffusion problems. *East West J. Numer. Math.*, 5 (4):291–311, 1997.

[58] D.L. Scharfetter and H.K. Gummel. Large signal analysis of a silicon Read diode oscillator. *IEEE Trans. Electron Devices*, ED-16:64–77, 1969.

[59] B. Straub, E. Meyer, and P. Fromherz. Recombinant maxi-K channels on transistor, a prototype of iono-electronic interfacing. *Nature Biotechnology*, 19:121–124, 2001.

[60] Y. Taur and T.H. Ning. *Fundamentals of modern VLSI devices*. Cambridge University Press, New York, NY, USA, 1998.

[61] R.S. Varga. *Matrix Iterative Analysis*. Englewood Cliffs, New Jersey, 1962.

[62] J. Xu and L. Zikatanov. A monotone finite element scheme for convection–diffusion equations. *Math. Comp.*, 68(228):1429–1446, 1999.

[63] G. Zeck and P. Fromherz. Noninvasive neuroelectronic interfacing with synaptically connected snail neurons on a semiconductor chip. *PNAS*, **98**:10457–10462, 2001.